Published in final edited form as:
*J Electron Spectros Relat Phenomena*. 2009 May 1; 172(1-3): 2–8. doi:10.1016/j.elspec.2009.02.008.

# Amine Terminated SAMs: Investigating Why Oxygen is Present in these Films

**J. E. Baio**[*], **T. Weidner**[*], **J. Brison**[*], **D.J. Graham**[**], **Lara J. Gamble**[*], and **David G. Castner**[*,§]

[*] National ESCA and Surface Analysis Center for Biomedical Problems, University of Washington, Departments of Bioengineering and Chemical Engineering, Box 351750, Seattle, WA 98195

[**] Asemblon, 15340 NE 92nd Street, Suite B, Redmond, WA 98052

## Abstract

Self-assembled monolayers (SAMs) on gold prepared from amine-terminated alkanethiols have long been employed as model positively charged surfaces. Yet in previous studies significant amounts of unexpected oxygen containing species are always detected in amine terminated SAMs. Thus, the goal of this investigation was to determine the source of these oxygen species and minimize their presence in the SAM. The surface composition, structure, and order of amine-terminated SAMs on Au were characterized by X-ray photoelectron spectroscopy (XPS), time-of-flight secondary ion mass spectroscopy (ToF-SIMS), sum frequency generation (SFG) and near edge X-ray absorption fine structure (NEXAFS) spectroscopy. XPS determined compositions of amine-terminated SAMs in the current study exhibited oxygen concentrations of 2.4 ± 0.4 atomic %, a substantially lower amount of oxygen than reported in previously published studies. High-resolution XPS results from the $S_{2p}$, $C_{1s}$ and $N_{1s}$ regions did not detect any oxidized species. Angle-resolved XPS indicated that the small amount of oxygen detected was located at or near the amine head group. Small amounts of oxidized nitrogen, carbon and sulfur secondary ions, as well as ions attributed to water, were detected in the ToF-SIMS data due to the higher sensitivity of ToF-SIMS. The lack of N-O, S-O, and C-O stretches in the SFG spectra are consistent with the XPS and ToF-SIMS results and together show that oxidation of the amine-terminated thiols alone can only account for, at most, a small fraction of the oxygen detected by XPS. Both the SFG and angle-dependent NEXAFS indicated the presence of gauche defects in the amine SAMs. However, the SFG spectral features near 2865 $cm^{-1}$, assigned to the stretch of the methylene group next to the terminal amine unit, demonstrate the SAM is reasonably ordered. The SFG results also show another broad feature near 3200 $cm^{-1}$ related to hydrogen-bonded water. From this multi-technique investigation it is clear that the majority of the oxygen detected within these amine-terminated SAMs arises from the presence of oxygen containing adsorbates such as tightly bound water.

## 1. Introduction

Self-assembled monolayers (SAMs) of alkanethiol molecules on metal surfaces (e.g., Au and Ag) have been extensively employed to control the composition and charge of surfaces1–3. These charged substrates have been used to drive the absorption of various biological materials

§Corresponding Author: David G. Castner, National ESCA and Surface Analysis Center for Biomedical Problems, Departments of Bioengineering and Chemical Engineering, Box 351750, Seattle, WA 98195, 1-206-543-8094 (phone), 1-206-543-3778 (fax), castner@nb.engr.washington.edu.

(proteins, cells, etc.)[4–9]. In particular, amine-terminated SAMs ($NH_2$-SAMs) have been used to model positively charged surfaces. However, unlike simple methyl terminated SAMs ($CH_3$-SAMs), the quality of $NH_2$-SAMs is more difficult to control. This difficulty is illustrated by the previously reported x-ray photoelectron spectroscopy (XPS) results from $NH_2$-SAMs, all of which describe an unusually high and unexpected concentration of oxygen within the monolayer (a pure amine-terminated thiol should not contain oxygen). Across a range of protocols, the amount of oxygen detected by XPS varies from 5–8 atomic %[4,5,10]. In contrast, XPS does not detect the presence of oxygen in solution assembled $CH_3$-SAMs[11].

There are two possible hypotheses that can explain the presence of oxygen within the $NH_2$-SAMs. The first is that the SAM is covered with oxygen containing coadsorbates[12,13], while the second assumes the nitrogen, carbon, or sulfur species within the $NH_2$-SAMs are oxidizing[10]. Even though there is a large body of work focused on various protocols that try to improve the quality of an $NH_2$-SAMs (to avoid double layers, control the charge of the terminal group, etc), no study has directly addressed the validity of either of these two hypotheses [4,10,14–16]. The inability to control the composition of these SAMs has implications for the studies where these substrates are used. The formation of oxidized carbon, nitrogen or sulfur species within the SAM will affect stability, while a layer of contamination could adversely affect the absorption of proteins or cells[12].

In this investigation these two hypotheses were tested using several complementary surface analysis techniques to characterize the $NH_2$-SAMs. The composition and oxidation state of each component within the monolayer was probed with XPS and static time-of-flight secondary mass spectroscopy (ToF-SIMS). Monolayer order and identification of potential coadsorbates was explored via angle resolved XPS (ARXPS) in conjunction with both sum frequency generation (SFG) and near edge x-ray absorption fine structure (NEXAFS) spectroscopy.

## 2. Experimental

### 2.1 Substrate preparation and assembly of amine-terminated thiols

Silicon substrates (Microelectronics Inc., San Jose, CA) were cleaned by sequential sonications in DI water, dichloromethylene, acetone, and methanol. In a high vacuum thermal evaporator (pressure below $1 \times 10^{-6}$ Torr) 1 cm × 1 cm silicon substrates were first coated with a thin layer of Ti (10nm) followed by a high purity (99.99%) Au layer (80nm).

The Au coated substrates were then submerged into a 0.5mM solution of 11-amino-1-undecanthiol, hydrochloride (Asemblon, Redmond, WA) in 200 proof ethanol (Decon Labs, King of Prussia, PA). The substrates were allowed to soak in this ethanol-thiol solution for at least 16 hrs. Following assembly, the substrates were removed from solution, rinsed with pure ethanol, and then vortexed within a 10% v/v $NH_4OH$-ethanol solution. Previous investigations have shown that a basic, 10% v/v $NH_4OH$-ethanol rinse reduces the presence of unbound 11-amino-1-undecanthiol molecules that tend to be susceptible to oxidation[4,14]. Following the rinsing, the samples were dried and stored under pure $N_2$. Unbound 11-amino-1-undecanthiol controls were created by pressing the pure thiolated powder onto double sided sticky tape (Scotch Double Linerless 665, St. Paul, MN) attached onto clean Si substrates.

$CH_3$-SAMs were assembled with a protocol similar to that used to assemble the $NH_2$-SAMs. Briefly, the Au substrates were soaked in a 1mM 1-dodecanethiol (Aldrich, St. Louis, MO) – ethanol solution for at least 16 hrs and then rinsed within pure ethanol.

### 2.2 X-ray photoelectron spectroscopy

The XPS determined $NH_2$-SAM composition was an average from three spots on each of eight distinct samples (a total of 24 analysis spots). The data was acquired on a Kratos AXIS Ultra

DLD instrument (Kratos, Manchester, England) in the hybrid mode using a 0° take-off angle (TOA) and a monochromatic Al $K\alpha_{1,2}$ X-ray source (hν=1486.6eV). Angle-resolved measurements were conducted at 0°, 55°, and 70° TOAs using the electrostatic mode. Here, the photoelectron TOA is defined as the angle between the surface normal and the axis of the analyzer lens. Atomic compositions were calculated from $C_{1s}$ and $Au_{4f}$ peak areas obtained from survey (0–1100eV), detail $O_{1s}$ (524–544eV), detail $N_{1s}$ (390–410eV), and detail $S_{2p}$ (155–173eV) spectra (analyzer pass energy=80eV) collected in the hybrid mode. Molecular environments of the samples were probed by collecting high-resolution (analyzer pass energy= 20eV) spectra from the $N_{1s}$, $C_{1s}$, and $S_{2p}$ regions. Energy scales were calibrated by normalizing the large $CH_x$ peak in the $C_{1s}$ region to 285.0eV and a linear background was subtracted for all peak quantifications. The peak areas were normalized by the manufacturer supplied sensitivity factors and surface concentrations were calculated using the Kratos Vision software.

The oxidation state of the monomer powder was explored via high-resolution scans from a SSI S-Probe XPS system (Surface Science Instruments, Mountain View, CA) using a monochromatic Al $K\alpha_{1,2}$ X-ray source (hν=1486.6eV). Charge neutralization was accomplished via an electron flood gun. High-resolution scans (analyzer pass energy= 50eV) of the $N_{1s}$, $C_{1s}$, and $S_{2p}$ regions were collected at a TOA of 55°.

### 2.3 Time-of-Flight Secondary Ion Mass Spectrometry

Negative and positive secondary ion spectra were collected with an ION-TOF TOF.SIMS 5–100 instrument (ION-TOF, Münster, Germany), using a pulsed 25keV $Bi_3^+$ primary ion beam under static conditions (primary ion dose < $10^{13}$ ions/$cm^2$). Spectra were collected from a 100μm ×100μm region and five spots on three replicate samples (15 spots total) were examined. Positive spectra were mass calibrated using the $CH_3^+$, $NH_4^+$, $C_3H_5^+$ and $Au^+$ peaks. Negative spectra were mass calibrated using the $CH^-$, $OH^-$, and $Au^-$ peaks. Secondary ions were collected over a range of 0–400 *m/z* at a mass resolution ($m/\Delta m$) between 4000–8000. In addition, mass calibration corrections were typically kept below 20 ppm. Secondary ion peak intensities, within each spectrum, were normalized by the total ion intensity of that spectrum.

### 2.4 Near-Edge X-ray Absorption Fine Structure Spectroscopy

NEXAFS spectra were taken at the National Synchrotron Light Source (NSLS) U7A beamline at Brookhaven National Laboratory, using an elliptically polarized beam with ~85% *p*-polarization. This beam line uses a monochromator with a 600 l/mm grating that provides a full-width at half-maximum (FWHM) resolution of ~0.15 eV at the carbon K-edge (285 eV). The monochromator energy scale was calibrated using the 285.35 eV $C_{1s} \rightarrow \pi^*$ transition[17] on a graphite transmission grid placed in the path of the X-rays. To eliminate the effect of incident beam intensity fluctuations and monochromator absorption features, nitrogen K-edge NEXAFS spectra were normalized by the signal from a dodecanethiol SAM and C K-edge spectra were normalized by the spectrum of a clean gold surface prepared by *in vacuo* evaporation of gold. Both reference and signal channels were divided by the beam flux during each respective data acquisition[18]. Partial electron yield was monitored by a detector with the bias voltage maintained at −150 V and −360 V for the C K-edge and N K-edge, respectively. Samples were mounted to allow rotation about the vertical axis to change the angle between the sample surface and the incident X-ray beam. The NEXAFS angle is defined as the angle between the incident X-ray beam and the sample surface.

### 2.5 SFG Setup and Data Acquisition

The SFG vibrational spectra were acquired on an EKSPLA instrument (EKSPLA, Vilnius, Lithuania) by overlapping visible and tunable IR laser pulses (25 ps) in time and space at incidence angles of 60° and 54°, respectively. The visible beam with a wavelength of 532 nm was delivered by an EKSPLA Nd:YAG laser operating at 50 Hz, which was also used to pump

an EKSPLA optical parametric generation/amplification and difference frequency unit based on barium boarate and $AgGaS_2$ crystals to generate tunable IR laser radiation from 1000 – 4000 $cm^{-1}$. The bandwidth was 1 $cm^{-1}$ for the visible pump pulses and 1 – 6 $cm^{-1}$ for the IR laser radiation (1 $cm^{-1}$ for 2750 – 3000 $cm^{-1}$ and 6 $cm^{-1}$ for higher and lower wave numbers). Both beams were unfocussed and had a diameter of approximately 2 mm at the sample. The energy for both beams was 160 μJ per pulse. The SFG signal generated at the sample was then analyzed by filters and a monochromator, detected with a gated photomultiplier tube and stored in a computer. The spectra were collected with 400 shots per data point in 4 $cm^{-1}$ increments. All spectra were recorded in the *ppp* (sum, visible, and infrared) polarization combination and were normalized by a reference SFG signal generated in a ZnS crystal.

The fitting routine for the SFG data[19] used the following expression for the SFG intensity:[20].

$$I_{SFG} \propto \left|\chi^{(2)}\right|^2 = \left|\chi_{NR}^{(2)} e^{i\varphi} + \sum_{\nu} \int_{-\infty}^{\infty} \frac{A_\nu e^{i\varphi} e^{-[\omega_L - \omega_\nu/\Gamma_\nu]^2}}{\omega_L - \omega_\nu + i\Gamma_\nu} d\omega_l \right|^2 \quad (1)$$

Here, $\chi_{NR}^{(2)}$ is the second order nonlinear susceptibility of the nonresonant background, $A_\nu$ is the strength of the νth vibrational mode, φ denotes the phase of the respective mode and $\omega_{IR}$ refers to the frequency of the incident IR field. The integral is over Lorentzian lines, centered at $\omega_L$ with a width $\tilde{A}_L$ having a Gaussian distribution. In the fits, the Lorentzian line widths were set to 2 $cm^{-1}$ and $\Gamma_\nu$ was allowed to vary since the two contributions to the total line width could not be separated within the accuracy of the measurements. Phase values are reported as relative values to the nonresonant gold background and identical phases were assumed for all methyl and methylene related stretches.

## 3. Results and Discussion

### 3.1 XPS analysis

Theoretically, XPS data from an $NH_2(CH_2)_{11}SH$ monolayer on gold should only contain carbon from the alkylchain (84.6%), nitrogen from the amine head group (7.7%), and sulfur of the thiol group at the tail (7.7%), as well as gold from the substrate. However, several groups have reported anomalies with amine-terminated monolayers, including XPS determined compositions that vary from these ideal values. Previously, Wang and coworkers reported a method to interrupt double layer formation between amine-terminated thiols. This protocol incorporated tri-ethylamine into the ethanol-thiol solution followed by a basic wash after assembly. However, they also reported XPS oxygen concentrations of 5.5 atomic % for these $NH_2$-SAMs[10]. Other studies, in an effort to reduce the amount of oxygen, have adjusted the pH of both the assembly and rinsing solution, yet they still reported O/C atomic ratios of >0.1 [4,5].

Average XPS determined compositions of $NH_2$-SAMs from this investigation are reported in Table 1. As typically seen for amine-terminated SAMs, the surface composition showed the presence of carbon, nitrogen, sulfur, oxygen, and gold (from the underlying substrate). Omitting the Au contribution (Table 1), two large differences between the theoretical and experimental compositions become clear. First, the atomic % of S is lower than expected and secondly, there is a significant amount of O within the SAM. The lower percentage of sulfur can be explained by attenuation of the sulfur signal due to inelastic scattering from the long hydrocarbon over layer[1]. This result supports the conclusion that a relatively ordered monolayer was formed. With regards to the oxygen concentration, in comparison to the previously published compositions (a reported range of 5–8 atomic % when gold is included

in the composition), the compositions reported here contain a substantially lower concentration of oxygen (2.4 ± 0.4 atomic %).

High-resolution $C_{1s}$ spectra collected from the $NH_2$-SAMs, yield peak envelopes made up of two distinct peaks, one at 285eV corresponding to the $CH_2$ alkyl chain backbone and a small shoulder at 286.6eV (see Figure 1 for a typical spectrum). This small peak is at a binding energy that can be attributed to either a N-C or C-O species[21].

Close examination of the high-resolution $C_{1s}$ spectrum from the thiol-monomer powder produces results that are identical to those from the SAM on Au (Figure 1). Again there are two peaks within the $C_{1s}$ region, one corresponding to the $CH_x$ species and the other corresponding to a C-N or C-O species. Theoretically, the C-N species should account for only $1/11^{th}$ or 9% of the total carbon species within the SAM. In actuality, this small shoulder accounts for 14 ± 2 % of the total area of the $C_{1s}$ peak envelope (Table 2) from the SAM on Au and 10% for the monomer powder. The difference between the theoretical and experimental percentage of the $NH_2$-SAM C-N peak could be due to the fact that the C-N species is at the top of the monolayer and its emitted photoelectron would be less attenuated than those emitted from the underlying methylene carbons. It also should be noted that no C=O peak at ~ 288.5eV corresponding to a primary amide group was detected in any of the high-resolution $C_{1s}$ spectra.

The high-resolution $N_{1s}$ spectra taken from the $NH_2$-SAMs on Au exhibited two distinct peaks (see Figure 2 for a typical spectrum) located at 399.5 eV and 401.4 eV. The first peak at 399.5 eV corresponds to the C-N species of the amine head group. The 401.4 eV binding energy of the other peak is consistent with that of a protonated amine group[22]. In contrast, the $N_{1s}$ spectrum of the thiol powder shows only a single peak at 401.4 eV. This is not unexpected since the thiol powder is in the salt form ($Cl^-$ $NH_3^+(CH_2)_{11}SH$). After assembly no Cl is detected in the XPS survey spectra. Thus, the Cl is removed from the $NH_2$-SAM surface during the rinsing step. However, the existence of two distinct peaks within the $N_{1s}$ spectrum of the $NH_2$-SAM illustrates the fact that a substantial portion of the amine head groups were converted to a neutral state during the assembly and rinsing process. After assembly, the area of the peak assigned to the protonated head group varied from sample to sample, ranging from 24 –35% of the total area of the $N_{1s}$ peak envelope.

The $S_{2p}$ high resolution spectra from the $NH_2$-SAM on Au shown in Figure 3 exhibits a single doublet with peaks at 162.0 and 163.5eV due to the presence of bound thiols[23]. No unbound or oxidized sulfur species were detected. Angle-resolved XPS was performed to determine the location of the oxygen within the $NH_2$-SAM. Data acquired at three different photoelectron TOAs (0°, 55°, and 75°) are summarized in Table 3. A TOA of 0° is normal to the surface and will have the largest sampling depth. As expected, the Au signal from the substrate is increasingly attenuated by the $NH_2$-SAM with increasing TOA. The atomic ratio of C to Au increases three-fold over this 75° span. At a TOA of 55°, the atomic ratio of C/Au is equal to 2.16. Previously, Graham described a linear relationship between chain length and the C/Au attenuation ratio for $CH_3$-SAMs of various chain lengths[24]. For a 12-carbon chain length $CH_3$-SAM, at a TOA of 55°, Graham reported an atomic ratio of C/Au of 1.9. The slightly larger Au attenuation observed from the $NH_2$-SAM is consistent with the presence of an ad-layer on that SAM. The ratio of N and O to Au in the $NH_2$-SAM is also seen to increase with increasing TOA. It should also be noted that the ratio of O/N remains constant at all three TOAs. This suggests that the N and O are co-located in the monolayer.

### 3.2 ToF-SIMS analysis

ToF-SIMS is a versatile tool that probes complex surfaces with a high degree of sensitivity and molecular specificity[25]. As a consequence of the increased sensitivity of ToF-SIMS relative to XPS, small peaks from oxidized carbon, nitrogen, and sulfur secondary species were

detected in both the positive and negative secondary ion spectra. The detection of oxidized secondary ions from SAMs on Au is common[26–28] and a list of these secondary ions can be found in Table 4. To investigate the source of the oxygen contamination within the $NH_2$-SAMs, we compared the normalized intensities of each oxidized fragment to those from a $CH_3$-SAM of the same chain length (Table 4). $CH_3$-SAMs were chosen for comparison because XPS does not detect oxygen in freshly prepared $CH_3$-SAMs.

The biggest variation within the ToF-SIMS data from the two types of SAMs stems from the differences in head group. This is illustrated by the large differences in peak intensities (16–40 fold) of oxygen and nitrogen containing secondary ions from the two SAMs. In addition, the peak intensities of oxidized sulfur secondary ions from the $NH_2$-SAMs are two times larger than those from the $CH_3$-SAMs. While these oxidized sulfur secondary ions are always observed in ToF-SIMS data from thiol based SAMs, one possible explanation for the increased intensities in the $NH_2$-SAMs is that these negatively charged oxidized sulfur species interact with the amine head group making it difficult to wash them away during the rinsing step[13]. Another possible explanation is that the rate of photooxidation of the $NH_2$-SAM could be higher due to the polarity of the amine head group and a lower degree of ordering of the SAM. Cooper and Leggett, in their studies of SAM photooxidation rates, proposed that a high degree of ordering would limit access of reactive oxygen species to the thiol group, thus limiting the rate of sulfur, nitrogen, or carbon photooxidation[28]. While the polarity of the head group or the lower degree of ordering could drive a higher rate of photoxidation, compared to $CH_3$-SAMs, these oxidized species are not detected by XPS and thus we believe cannot be the major source of the oxygen contamination

At low masses there are $O^-$ and $OH^-$ peaks in the negative spectra as well as $H_3O^+$ in the positive spectra that can be attributed to the presence of water. The relative peak intensities of these secondary ions from the $NH_2$-SAMs are 3–7 times larger than the peak intensities observed for the hydrophobic $CH_3$-SAM, suggesting a greater amount of water is present on the $NH_2$-SAM.

### 3.3 NEXAFS Spectroscopy

NEXAFS spectroscopy can provide structural information about the molecular alignment in SAMs by measuring the angle dependence of the absorption peak intensities in spectra acquired at x-ray incidence angles from normal to glancing. The peaks present in the NEXAFS spectra also provide information about the chemical identity and bonding of surface species. N K-edge spectra of $NH_2$-SAMs acquired at NEXAFS angles of 70°, 55° and 20° are presented in Figure 4 along with the difference between the 70° and 20° spectra. The spectra are dominated by a broad σ* resonance near 406 eV related to the N-C bond. This peak is accompanied by an intense absorption resonance at 400.6 eV which can be assigned either to amide or primary amine ($-NH_2$) moieties.29–31 The latter possibility is more likely here since there is no evidence for C=O bonds in the NEXAFS C K-edge spectra (see below) or XPS $C_{1s}$ spectra (see section 3.1). The low-intensity pre-edge feature visible around 398 eV has been hypothesized to result from a hybridized or dissociated state of ammonia[32]. Other groups have proposed that a positively charged form of amine may be found at a different energy than the neutral form of the amine31. Since XPS results have shown a significant portion of the $NH_2$-SAM monolayer has a $-NH_3^+$ character, this peak may be due to the positively charged form of the amine group ($-NH_3^+$). Since radiation damage from the X-rays also becomes visible in this spectral range, a careful beam damage study was performed to rule out this possibility[33]. The spectra exhibit a weak but discernible negative dichroism for the amine transition, indicating a small degree of orientational order for this species. In addition, the negative sign of the observed difference peak suggests an upright orientation of the C-N bond for this group[18].

The C K-edge NEXAFS spectra are consistent with conclusions determined from the N K-edge spectra. Figure 5 shows the 55° x-ray incidence angle spectrum ("magic angle" spectrum) and a difference spectrum (70° - 20°) for the $NH_2$-SAM as well as corresponding reference $CH_3$-SAM spectra. The 55° spectra of the amine and the methyl SAMs are very similar. Both exhibit the expected resonances at ~287.7 eV (R*/C-H σ*), ~293.3 eV (C-C σ*) and 301.3 eV (C-C′ σ*)[18,34–36]. A very weak peak at ~285.2 eV is also observed and is tentatively assigned to an excitation into the alkane-metal orbitals, small amounts of contaminants present on the upstream gold grid used for beam current normalization, or a combination of both effects[37,38]. We performed a radiation damage study to rule out the possibility of beam damage as a cause for this feature[33]. Note, that a C=O related resonance expected near 288.5 eV[18,37,39] is not visible in the $NH_2$-SAM spectrum, consistent with no detectable C=O related peak in the XPS $NH_2$-SAM $C_{1s}$ spectrum. Thus, the C K-edge NEXAFS spectrum provides further evidence that conversion of the amine group to an amide group can't account for the O contamination detected by XPS. Also the lack of C=O resonance in the C K-edge spectrum is consistent with the interpretation that the 400.6 eV feature observed in the N K-edge spectrum is due to an amine species.

The polarization dependence displayed as the 70° - 20° difference spectra (Figure 5) is very similar in both the $NH_2$- and $CH_3$-SAMs, with the R* and σ* resonances exhibiting positive and negative anisotropy, respectively. The $NH_2$-SAM shows a weaker dichroism compared to the $CH_3$-SAM. The molecular orbitals related to the R* transition are oriented relatively perpendicular to the alkyl chain axis while those related to transitions into the C-C and C-C′ σ* orbitals are oriented more parallel to the chain axis. Consequently, the data indicates that both the $NH_2$- and the $CH_3$-SAMs are oriented upright (i.e., away from the Au substrate)[18]. The weaker dichroism of the $NH_2$-SAM can be explained either by a stronger inclination of the alkyl chains, a lower degree of structural order, or a combination of both.

### 3.4 SFG Spectroscopy

SFG spectra of the $NH_2$-SAM and a reference $CH_3$-SAM along with the corresponding fits are shown in Figure 6. The $CH_3$-SAM spectrum exhibits the expected resonances for the three peaks assigned to the terminal methyl unit at 2969 $cm^{-1}$ ($r^-$), 2936 $cm^{-1}$ ($r^-_{FR}$), and 2882 $cm^{-1}$ ($r^+$). These three resonances are observed on well ordered and densely packed SAMs. There are no $CH_2$ related stretching resonances visible in the spectrum, indicating that the alkyl chains are predominantly in an all-trans conformation[40]. Conversely, the $NH_2$-SAM spectrum is dominated by $CH_2$ related stretching vibrations in the region below 3000 $cm^{-1}$. A strong resonance observed near 2929 $cm^{-1}$ is commonly assigned to asymmetric stretching vibrations of methylene ($d^-$) and it indicates a significant amount of trans-gauche defects in the alkyl chains[7,40]. This agrees well with the NEXAFS C K-edge data where the $NH_2$-SAM exhibits a lower linear dichroism compared to the $CH_3$-SAM. Thus, both NEXAFS and SFG suggest the alkyl chains in the $NH_2$-SAM have a lower degree of structural order. The spectral feature near 2865 $cm^{-1}$ has been observed in $NH_2$-SAMs previously and assigned to the methylene group next to the terminal $NH_2$ unit ($d^+_w$)[7,40]. This peak indicates that the SAM surface is still reasonably ordered in spite of the trans-gauche defects in the chain since an SFG peak would not be observed if this group was randomly oriented.

The region above 3000 $cm^{-1}$ is dominated by a broad OH resonance near 3200 $cm^{-1}$ related to strongly hydrogen-bonded water ("ice-like" water)[41], and is also observed on peptide films where $NH_2$ terminated lysine side chains are exposed to water[42]. The presence of bound water in the SFG spectrum is consistent with the observation of water related fragments in ToF-SIMS data. Spectral features at 3333 $cm^{-1}$ and 3247 $cm^{-1}$ are assigned to the asymmetric ($d^-$) and symmetric ($d^+$) N-H stretches of the terminal $NH_2$ unit, respectively. Previous SFG studies have observed NH stretches from amine groups in this spectral range[42,43]. The mode observed

near 3020 $cm^{-1}$ is more difficult to assign. It could be related to symmetric or asymmetric stretching modes of $NH_3^+$.

## 4. Concluding Remarks

The aim of this investigation was to use complementary surface analysis techniques to investigate the source of the oxygen contamination found within $NH_2$-SAMs and minimize its presence. NEXAFS and SFG experiments did indicate the presence of gauche defects in the alkyl chains, yet, other spectral features pointed to a reasonably ordered surface. While it has been shown that these defects could allow oxygen to penetrate the SAM and interact/oxidize with the thiol molecule, XPS did not detect the presence of any oxidized sulfur or nitrogen species. ToF-SIMS, with its higher sensitivity, did detect the presence of some fragments containing both oxygen and nitrogen, but XPS, NEXAFS and SFG did not detect any peaks that could be attributed to amide groups. Thus, as the concentration of oxidized sulfur and amine species were below the XPS detection limits this indicates that oxidized sulfur and amine species are not the major contributors to the oxygen contamination observed for the $NH_2$-SAMs in this study. Angle-resolved XPS experiments show that the oxygen is co-located with the amine head group. In addition, ToF-SIMS and SFG results suggest that there is a measurable amount of water bound to the surface. Thus, we believe that the majority of the oxygen detected within these amine SAMs most likely arises from the presence of oxygen containing coadsorbates such as tightly bound water.

## Acknowledgments

This research was supported by NIH grants EB-002027, EB-006163 and GM-074511. TW thanks the Deutsche Forschungsgemeinschaft for a research fellowship. We thank Daniel Fischer (NIST) and Cherno Jaye (Hunter College) for providing us with the experimental equipment for NEXAFS spectroscopy and their help at the synchrotron. NEXAFS studies were performed at the NSLS, Brookhaven National Laboratory, which is supported by the U.S. Department of Energy, Division of Materials Science and Division of Chemical Sciences.

## References

1. Bain CD, Evall J, Whitesides GM. Journal of the American Chemical Society 1989;111:7155–7164.
2. Ostuni E, Yan L, Whitesides GM. Colloids and Surfaces B-Biointerfaces 1999;15:3–30.
3. Wink T, vanZuilen SJ, Bult A, vanBennekom WP. Analyst 1997;122:R43–R50.
4. Wang H, Castner DG, Ratner BD, Jiang SY. Langmuir 2004;20:1877–1887. [PubMed: 15801458]
5. Chuang WH, Lin JC. Journal of Biomedical Materials Research Part A 2007;82A:820–830. [PubMed: 17326142]
6. Faucheux N, Schweiss R, Lutzow K, Werner C, Groth T. Biomaterials 2004;25:2721–2730. [PubMed: 14962551]
7. Palyvoda O, Bordenyuk AN, Yatawara AK, McCullen E, Chen CC, Benderskii AV, Auner GW. Langmuir 2008;24:4097–4106. [PubMed: 18338909]
8. Schilp S, Ballav N, Zharnikov M. Angewandte Chemie-International Edition 2008;47:6786–6789.
9. Ballav N, Schilp S, Zharnikov M. Angewandte Chemie-International Edition 2008;47:1421–1424.
10. Wang H, Chen SF, Li LY, Jiang SY. Langmuir 2005;21:2633–2636. [PubMed: 15779923]
11. Graham DJ, Price DD, Ratner BD. Langmuir 2002;18:1518–1527.
12. Sprik M, Delamarche E, Michel B, Rothlisberger U, Klein ML, Wolf H, Ringsdorf H. Langmuir 1994;10:4116–4130.
13. Sahoo RR, Patnaik A. Applied Surface Science 2005;245:26–38.
14. Li LY, Chen SF, Jiang SY. Langmuir 2003;19:3266–3271.
15. Fears KP, Creager SE, Latour RA. Langmuir 2008;24:837–843. [PubMed: 18181651]
16. Wallwork ML, Smith DA, Zhang J, Kirkham J, Robinson C. Langmuir 2001;17:1126–1131.
17. Batson PE. Physical Review B 1993;48:2608.

18. Stöhr, J. NEXAFS Spectroscopy. Vol. 25. Springer-Verlag; Berlin: 1992.
19. Moore FG, Becraft KA, Richmond GL. Applied Spectroscopy 2002;56:1575–1578.
20. Bain CD. J Chem Soc, Faraday Trans 1995;91:1281–1296.
21. Michel R, Subramaniam V, McArthur SL, Bondurant B, D'Ambruoso GD, Hall HK, Brown MF, Ross EE, Saavedra SS, Castner DG. Langmuir 2008;24:4901–4906. [PubMed: 18393486]
22. Ratner BD, Castner DG. Biomaterials 1990;11:143–146.
23. Castner DG, Hinds K, Grainger DW. Langmuir 1996;12:5083–5086.
24. Graham, DJ. PhD Dissertation. University of Washington; 2001.
25. Belu AM, Graham DJ, Castner DG. Biomaterials 2003;24:2625–2653.
26. Graham DJ, Ratner BD. Langmuir 2002;18:5861–5868.
27. Hutt DA, Leggett GJ. Journal of Physical Chemistry 1996;100:6657–6662.
28. Cooper E, Leggett GJ. Langmuir 1998;14:4795–4801.
29. Cooper G, Gordon M, Tulumello D, Turci C, Kaznatcheev K, Hitchcock AR. Journal of Electron Spectroscopy and Related Phenomena 2004;137:795–799.
30. Gordon ML, Cooper G, Morin C, Araki T, Turci CC, Kaznatcheev K, Hitchcock AP. Journal of Physical Chemistry A 2003;107:6144–6159.
31. Zubavichus Y, Zharnikov M, Schaporenko A, Grunze M. Journal of Electron Spectroscopy and Related Phenomena 2004;134:25–33.
32. Ozawa K, Hasegawa T, Edamoto K, Takahashi K, Kamada M. J Phys Chem B 2002;106:9380–9386.
33. For the beam damage study at the N K-edge, the 388 eV to 410 eV energy range was repeatedly scanned and analyzed. In addition, the partial electron yield at 398 eV was monitored over time to rule out damage related changes in the first seconds. No changes in the spectra were observed within 15 minutes, which is more than the exposure time in the longest nitrogen scans performed within this work. An analogous radiation damage study for the C *K*-edge proved that the pre-edge feature observed near 285.2 eV is not caused by beam damage.
34. Outka DA, Stöhr J, Rabe JP, Swalen JD. Journal of Chemical Physics 1988;88:4076.
35. Weiss K, Bagus PS, Wöll C. Journal of Chemical Physics 1999;111:6834.
36. Väterlein P, Fink R. Journal of Chemical Physics 1998;108:3313.
37. Cabarcos OM, Shaporenko A, Weidner T, Uppili S, Dake LS, Zharnikov M, Allara DL. J Phys Chem C 2008;112:10842–10854.
38. Witte G, Weiss K, Jakob P, Braun J, Kostov KL, Wöll C. Physical Review Letters 1998;80:121.
39. Ballav N, Schupbach B, Dethloff O, Feulner P, Terfort A, Zharnikov M. J Am Chem Soc 2007;129:15416–15417. [PubMed: 18041835]
40. Himmelhaus M, Eisert F, Buck M, Grunze M. J Phys Chem B 2000;104:576–584.
41. Du Q, Freysz E, Shen YR. Science 1994;264:826–828. [PubMed: 17794723]
42. Mermut O, Phillips DC, York RL, McCrea KR, Ward RS, Somorjai GA. J Am Chem Soc 2006;128:3598–3607. [PubMed: 16536533]
43. Jung SY, Lim SM, Albertorio F, Kim G, Gurau MC, Yang RD, Holden MA, Cremer PS. J Am Chem Soc 2003;125:12782. [PubMed: 14558825]

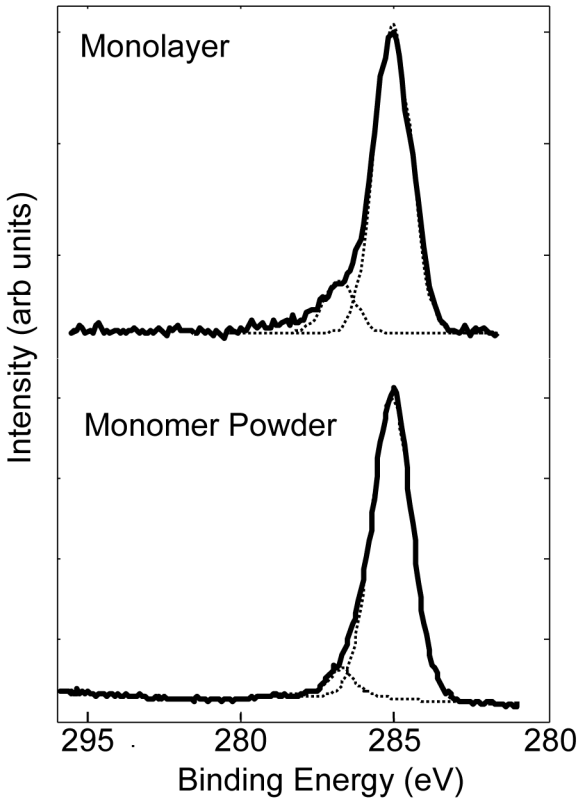


**Figure 1.**
High-resolution XPS $C_{1s}$ spectra of the $Cl^{-}NH_3^{+}(CH_2)_{11}SH$ powder (bottom) and the $NH_2$-SAM on Au (top). In both cases the spectra have peaks at 285eV ($CH_x$) and 286.6eV (C-N/C-O).

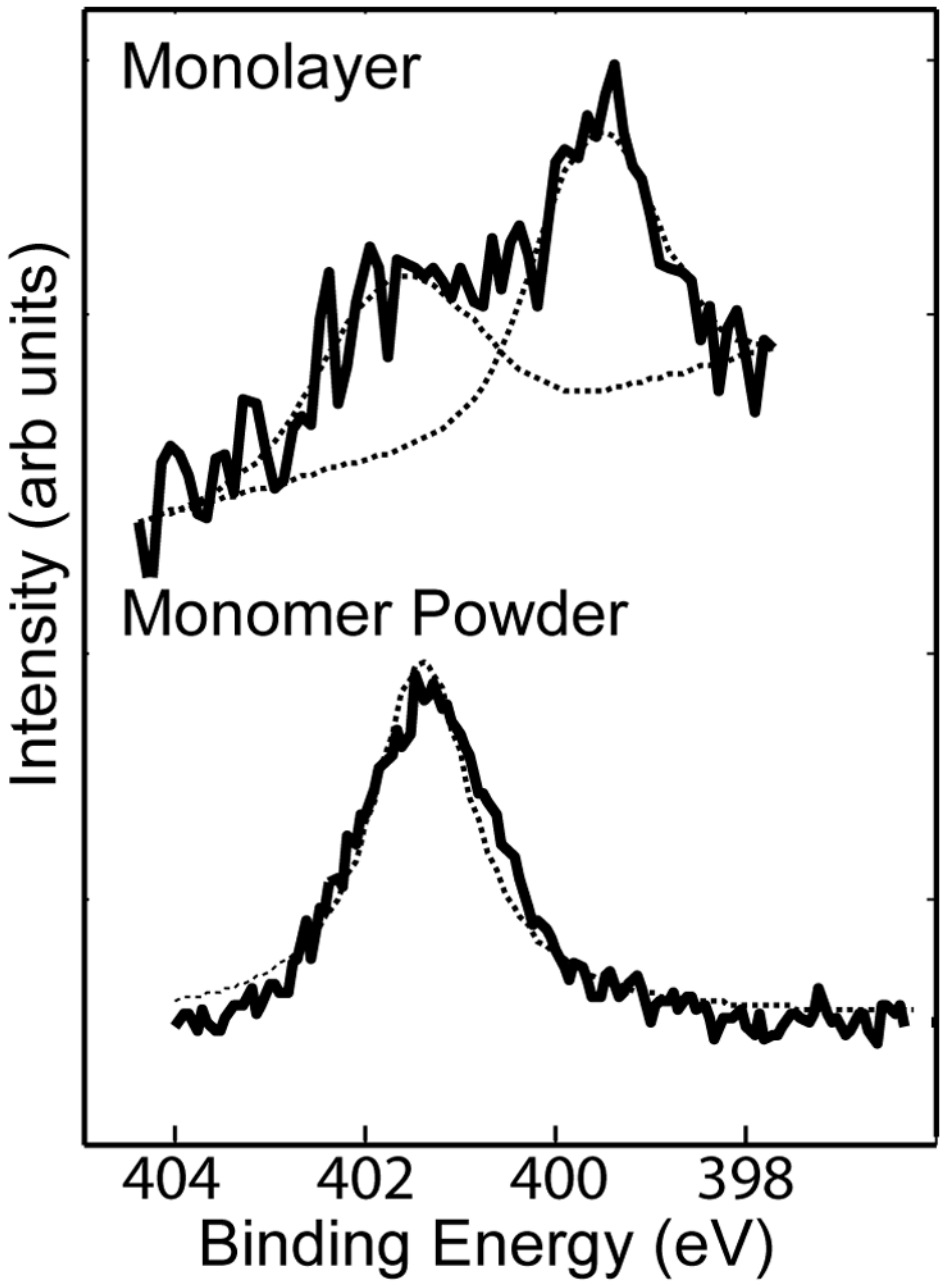


**Figure 2.**
High-resolution XPS $N_{1s}$ spectra of the $Cl^{-}NH_3^{+}(CH_2)_{11}SH$ powder (bottom) and the $NH_2$-SAM on Au (top). The powder spectrum has a single peak at 401.4eV (protonated amine). The $NH_2$-SAM on Au spectrum has peaks at 399.5eV (C-N) and 401.4 eV (protonated amine).

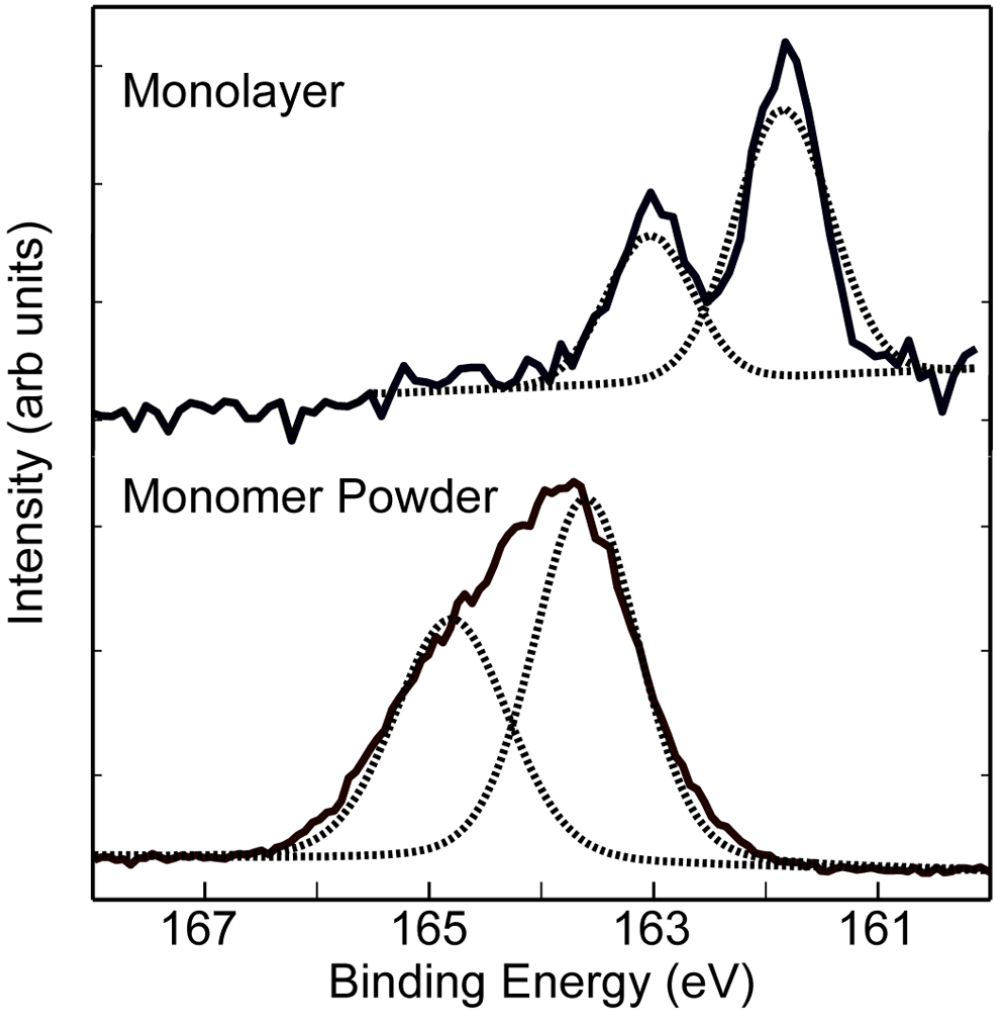


**Figure 3.**
High-resolution XPS $S_{2p}$ spectra of the $Cl^{-}NH_3^{+}(CH_2)_{11}SH$ powder (bottom) and the $NH_2$-SAM on Au (top). Each spectrum was fit using one $S_{2p}$ doublet with a splitting of 1.2eV.

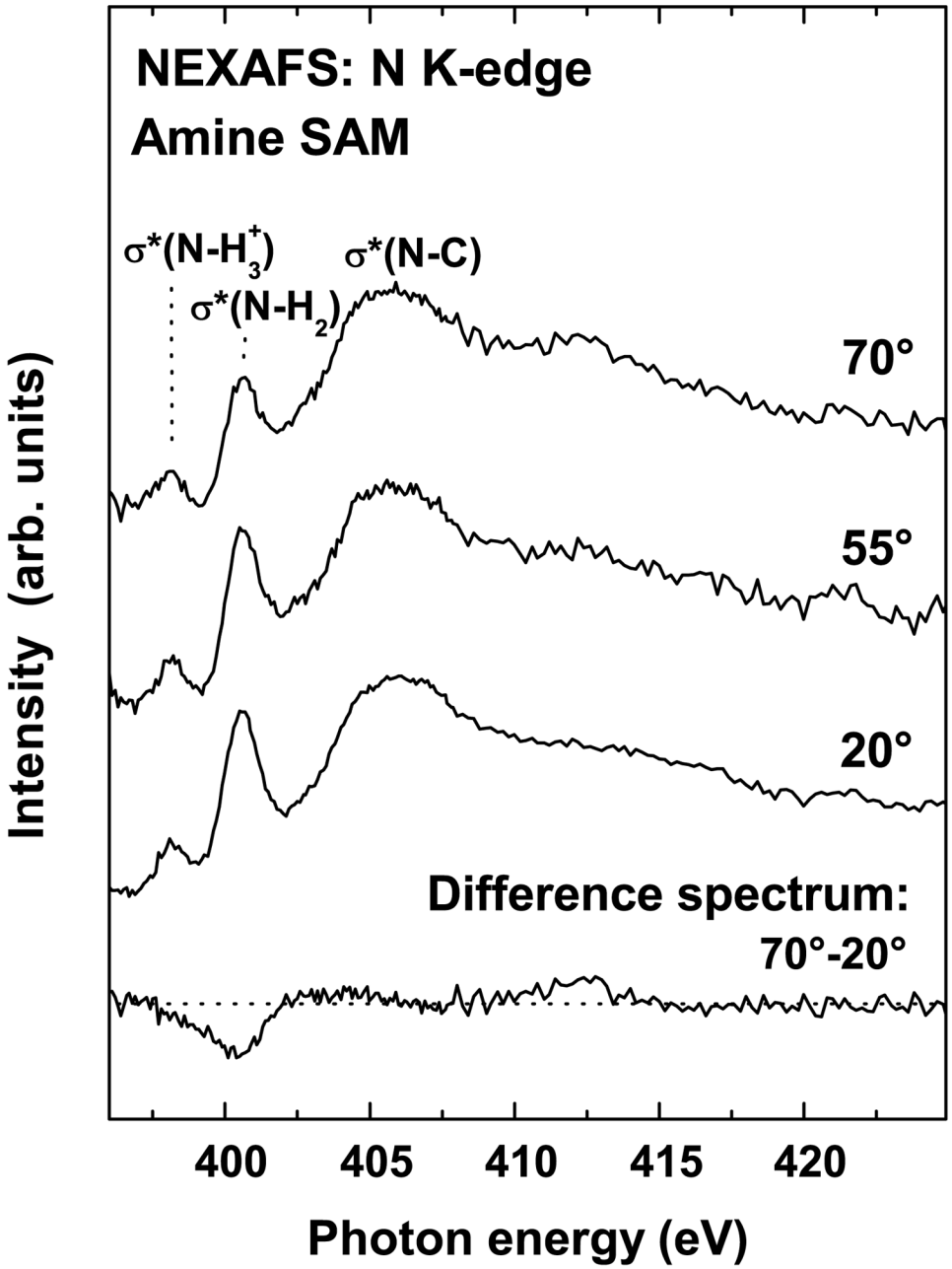


**Figure 4.**
NEXAFS spectra of the nitrogen *K*-edge for amine SAMs acquired at angles of 70°, 55° and 20° along with the 70 and the 20° difference spectrum.

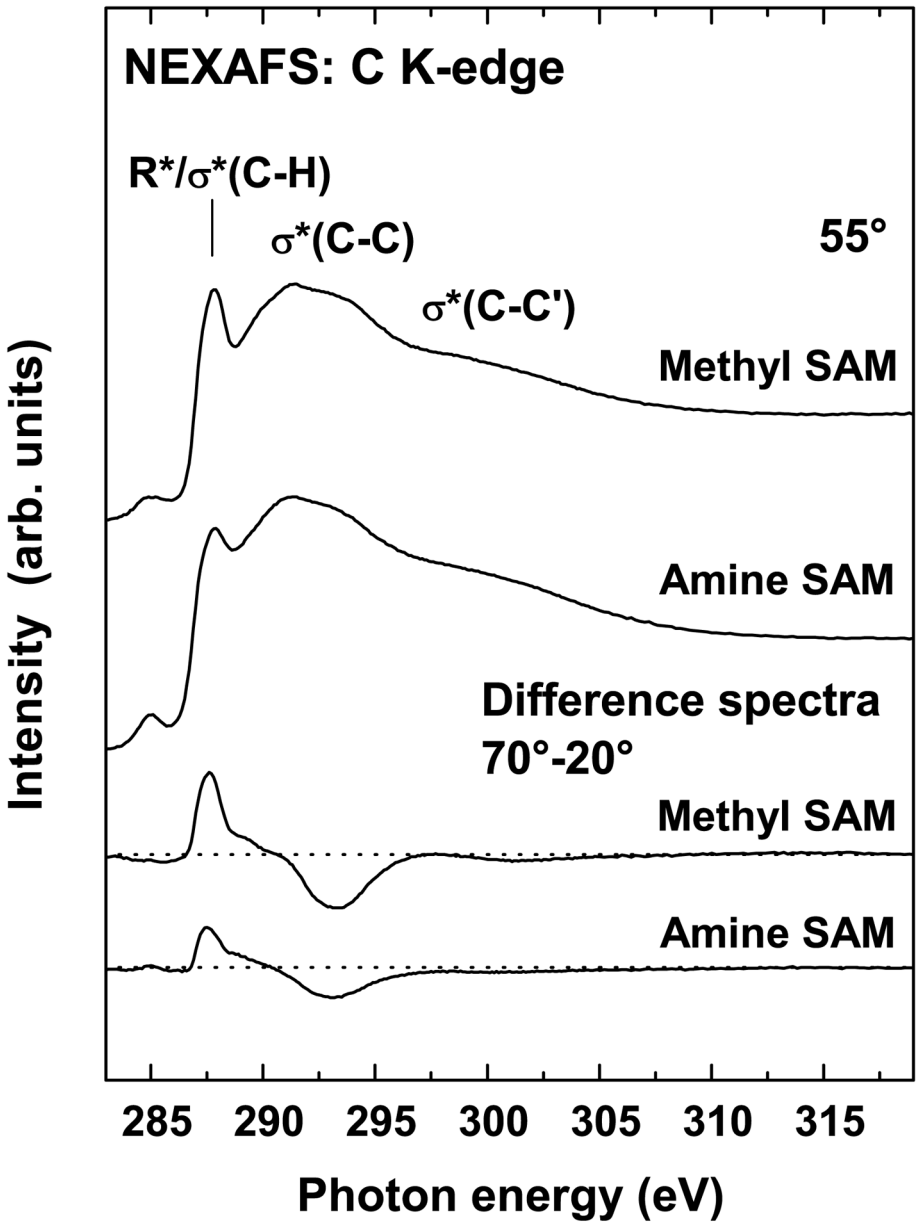


**Figure 5.**
NEXAFS spectra of the carbon *K*-edge for the $NH_2$- and $CH_3$-terminated SAMs acquired at 55° along with their respective difference spectra (70°-20°).

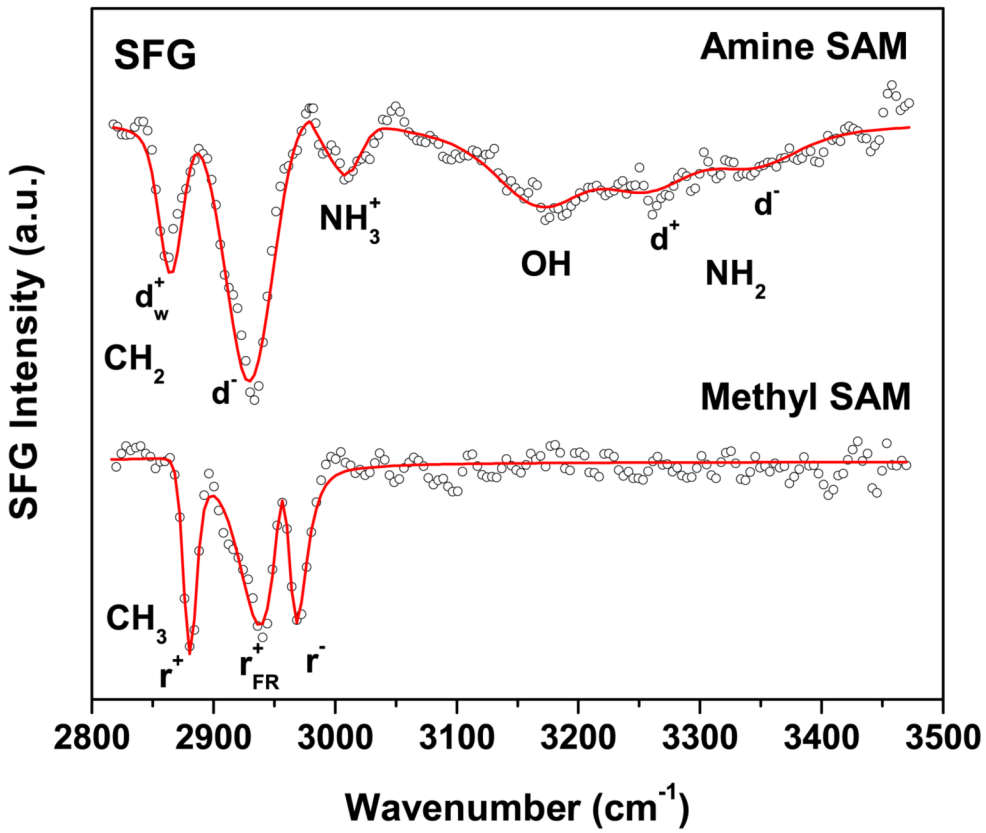


**Figure 6.**
SFG spectrum of $NH_2$- (upper trace) and $CH_3$-terminated (lower trace) SAMs on gold. Solid lines are best fits based on equation 1.

**Table 1**

Summary of XPS determined elemental compositions.

| | Au | C | O | N | S |
|---|---|---|---|---|---|
| **Theoretical Composition** | **--** | **84.6** | **--** | **7.7** | **7.7** |
| **Experimental Composition*** | **39.2** | **53.0** | **2.4** | **3.6** | **1.8** |
| Std dev | 1.9 | 2.0 | 0.4 | 0.3 | 0.2 |
| **Experimental Composition w/o Au** | **-** | **87.2** | **4** | **5.9** | **2.9** |
| Std dev | - | 0.9 | 0.6 | 0.6 | 0.3 |

*Average experimental composition from eight distinct samples (three spots per sample).

All data were collected at a 0° TOA in the hybrid mode.

## Table 2

High-resolution XPS $C_{1s}$ peak fit results for the $NH_2$-SAM on Au.

| | **C-$H_x$ (285eV)** | **C-N/C-O (286.6eV)** |
|---|---|---|
| **Theory** | **91**% | **9**% |
| **Experimental Composition*** | **86**% | **14**% |
| Std dev | 2% | 2% |

*Average experimental composition from eight distinct samples (three spots per sample).

All data were collected at a 0° TOA in the hybrid mode.

**Table 3**

Angle-resolved XPS determined elemental compositions of $NH_2$-SAMs on Au.

| | Atomic % (StdDev)* | | | | |
|---|---|---|---|---|---|
| **TOA** | **Au** | **C** | **O** | **N** | **S** |
| 0 | 41.1 (2.5) | 49.9 (2.5) | 3.1 (0.3) | 4.2 (0.5) | 1.7 (0.1) |
| 55 | 28.5 (2.4) | 61.7 (2.7) | 3.4 (0.6) | 4.7 (0.4) | 1.8 (0.1) |
| 75 | 17.3 (1.3) | 70.2 (1.4) | 4.7 (0.6) | 5.9 (0.6) | 1.8 (0.1) |

| | Atomic % Ratios (StdDev)* | | | | |
|---|---|---|---|---|---|
| **TOA** | **C/Au** | **N/Au** | **S/Au** | **O/Au** | **O/N** |
| 0 | 1.21 (0.10) | 0.10 (0.01) | 0.04 (0.00) | 0.08 (0.01) | 0.75 (0.11) |
| 55 | 2.16 (0.21) | 0.16 (0.02) | 0.06 (0.01) | 0.12 (0.02) | 0.71 (0.13) |
| 75 | 4.05 (0.31) | 0.34 (0.04) | 0.10 (0.01) | 0.27 (0.04) | 0.79 (0.12) |

*Average experimental composition from three distinct samples (one spot per sample). All data were taken at 0°, 55°, and 75° takeoff angles in the electrostatic mode. Note: the takeoff angle is defined as the angle between the surface normal and the analyzer.

## Table 4

ToF-SIMS peak intensity ratios for selected oxygen containing peaks detected on $NH_2$- and $CH_3$-SAMs.*

| Ion | Mass | RATIO $NH_2$-SAM/$CH_3$-SAM |
|---|---|---|
| $O^-$ | 15.995 | 6.7 |
| $OH^-$ | 17.0029 | 3.2 |
| $CHO^-$ | 29.0034 | 7.9 |
| $C_2O^-$ | 39.9959 | 6.5 |
| $C_2HO^-$ | 41.0043 | 5.9 |
| $CNO^-$ | 41.9999 | 30.5 |
| $CHNO^-$ | 43.0027 | 29.5 |
| $C_2HO^-$ | 43.0207 | 4.6 |
| $CO_2^-$ | 43.9917 | 3.2 |
| $CHO_2^-$ | 45.0002 | 6.2 |
| $SO^-$ | 47.9702 | 2.5 |
| $SOH^-$ | 48.9777 | 1.9 |
| $H_2O_3^-$ | 50.0045 | 13.2 |
| $C_3O^-$ | 51.9977 | 8.4 |
| $C_3HO^-$ | 53.0055 | 6.0 |
| $C_3H_3O^-$ | 55.0223 | 10.2 |
| $C_3H_5O^-$ | 57.038 | 6.7 |
| $CHSO^-$ | 60.9778 | 3.2 |
| $SO_2^-$ | 63.9656 | 2.0 |
| $SO_3^-$ | 79.9625 | 2.7 |
| $SO_4^-$ | 95.9617 | 0.8 |
| $S_2O_3^-$ | 111.9358 | 2.6 |
| $AuSO^-$ | 244.9287 | 1.3 |
| $H_3O^+$ | 19.0185 | 3.4 |
| $CHO^+$ | 29.0027 | 5.1 |
| $CH_3O^+$ | 31.0191 | 5.4 |
| $C_2H_2O^+$ | 42.008 | 2.2 |
| $CH_2NO^+$ | 44.0144 | 7.7 |
| $CH_4NO^+$ | 46.029 | 40.3 |
| $C_3H_3O^+$ | 55.0317 | 2.7 |
| $C_2H_6NO^+$ | 60.046 | 16.5 |
| $SO_2H^+$ | 64.9708 | 1.8 |
| $H_2SO_4^+$ | 97.9758 | 5.5 |

*Intensities for each peak were normalized to the total intensity of the corresponding spectrum. Ratios presented here are calculated from average normalized peak intensities taken from five different spots on three samples of each SAM.